SKA1 ERROR BUDGETS

Document number SKA-TEL-SKO-0000641
Context .... SKA-OFFICE-SCI-ERB
Revision 01
Author .... SKAO Science Team
Date 2016-09-06
Document Classification .... UNRESTRICTED
Status .... Released

Name	Designation	Affiliation	Signature	
Authored by:				
SKAO Science Team p.p. Robert Braun	Science Director	SKAO		
			Date:	Sep 8, 2016
Owned by:				
Robert Braun	Science Director	SKAO		
			Date:	Sep 8, 2016
Approved by:				
Robert Braun	Science Director	SKAO		
			Date:	Sep 8, 2016
Released by:				
Alistair McPherson	Head of Project	SKAO	A M McPherson	
			Date:	Sep 8, 2016

DOCUMENT HISTORY

Revision	Date Of Issue	Engineering Change Number	Comments
01	2016-09-06	-	First release of document

DOCUMENT SOFTWARE

	Package	Version	Filename
Word processor	MS Word	Word 2007	SKA-TEL-SKO-0000641-SKA1ErrorBudgets
Block diagrams			
Other			

ORGANISATION DETAILS

Name	SKA Organisation
Registered Address	Jodrell Bank Observatory Lower Withington Macclesfield Cheshire SK11 9DL United Kingdom Registered in England & Wales Company Number: 07881918
Fax.	+44 (0)161 306 9600
Website	www.skatelescope.org

TABLE OF CONTENTS

LIST OF FIGURES

LIST OF TABLES

LIST OF ABBREVIATIONS

AIP .... Advanced Instrumentation Programme
BD .... SKA1 Baseline Design
DM.......................... Dispersion Measure
EMI......................... Electromagnetic Interference
EoR .... Epoch of Reionisation
FRB........................ Fast Radio Burst
FWHM.................... Full Width Half Maximum
HPSO..................... High Priority Science Objective
ISW .... Integrated Sachs Wolfe effect
NIP .... Non-image Processing
PSF .... Point Spread Function
RFI .... Radio Frequency Interference
RM.......................... Rotation Measure
RMS .... Root Mean Square
SEFD...................... System Equivalent Flux Density
SKA........................ Square Kilometre Array
SKAO .... SKA Organisation
VLBI .... Very Long Baseline Interferometry

1 Introduction

1.1 Purpose of the document

This document is intended to provide high level constraints that need to be jointly satisfied by the SKA instrument design together with its calibration strategy in order to meet the most demanding scientific performance goals.

1.2 Scope of the document

A parametric error budget analysis is applied to the SKA1-Mid and SKA1-Low facilities under conditions that simulate long observations. Only a subset of all relevant factors, namely those pertaining to imaging artefacts and incomplete calibration, are considered here. The analysis is put into context by also considering the most relevant comparison facilities that are currently in operation. The practical implications of the analysis are briefly summarised.

2 References

2.1 Applicable documents

The following documents are applicable to the extent stated herein. In the event of conflict between the contents of the applicable documents and this document, **the applicable documents** shall take precedence.

[AD1] –

2.2 Reference documents

The following documents are referenced in this document. In the event of conflict between the contents of the referenced documents and this document, **this document** shall take precedence.

[RD1] SKA-TEL-SKO-0000007-Rev02, SKA1 Level 0 Science Requirements
[RD2] SKA-TEL-SKO-DD-001, SKA1 Baseline Design version 2
[RD3] Braun, R., 2013, A&A 551, A91, "Understanding synthesis imaging dynamic range"
[RD4] Fernandez, X., et al. 2013, ApJL 770, L29, "A pilot for a VLA HI Deep Field"
[RD5] Owen, F.N., Morrison, G.E., 2008, AJ 136, 1889, "The deep SWIRE field: 20cm continuum radio observations: A crowded sky"
[RD6] Yatawatta, S., et al. 2013, A&A 550, 136, "Initial deep LOFAR observations of epoch of reionization windows. I. The north celestial pole"

3 Introduction

The SKA Observatory is being designed to enable a variety of extremely challenging scientific goals to be achieved. A good summary of the scientific needs is given in Table 1 of Appendix A within the top level Science Requirements [RD1]. Extremely high values of the spectral, polarisation and brightness dynamic range (quantities that are defined in that document) must be achieved to allow the science objectives to be realised. What this implies in practise is that even extremely long integrations (as long as 2000 hours per pointing) must still achieve essentially the theoretical thermal noise level, and not be limited by other effects. This is an extremely challenging goal and one that is particularly difficult to verify in advance within a design. Subtle systematic errors may only become apparent after ten, one hundred or even one thousand hours of integration time. Predicting which effects might become dominant as longer integrations are accumulated and how such effects might be mitigated requires a deep understanding of the telescope system and its environment. Such predictions can ultimately only be tested by undertaking the actual observations, which may require years of operation. Simulations can be helpful in gaining confidence in a design, but are only as useful as they are complete in realistically capturing all relevant effects.

A framework for the quantified analysis of many potential limitations to the scientific performance of telescope systems has been given in RD3. Three basic categories of limitations are identified there: 1. instrumental artefacts; 2. imaging artefacts; 3. incomplete calibration of the instrumental response. As noted in RD3: “The first category can be addressed by insuring a linear system response to signal levels together with other design measures within the receiver and correlator systems that minimise spurious responses. While challenging to achieve, the engineering requirements in this realm are moderately well defined and this class of circumstance will not be considered further in the current discussion.” The two remaining error categories jointly contribute to a variety of potential limitations. RD3 break these down into six distinct error terms, each described by a parametric model that expresses the visibility or image noise as function of the amplitude of an instrumental parameter. In this document we will apply that analysis to the current SKA1-Mid and SKA1-Low designs to provide guidance on the precision with which relevant system parameters must be calibrated in order for them not to become impediments to the science performance of long integrations.

Table 1. Parameter definitions.

Parameter	Definition
φ_C	Main beam “external” gain calibration error
η_F	Far sidelobe suppression factor
ε_F	Far sidelobe attenuation relative to on-axis
ε_S	Near-in sidelobe attenuation relative to on-axis
ε_M	Discrete source modelling error
P (arcs)	Mechanical slowly varying systematic pointing error
τ_P (min)	Timescale for slowly varying pointing error
ε'_P	Rapidly varying random pointing induced gain error
τ'_P (sec)	Timescale for rapid pointing errors
ε_Q	Main beam shape asymmetry
ε_B	Main beam shape modulation with frequency
l_C (m)	Effective “cavity” dimension for frequency modulations of main beam
τ^*	Nominal self-cal solution timescale (10% PSF smearing at first null)
$\Delta\nu^*$	Nominal self-cal solution bandwidth (10% PSF smearing at first null)

σ_{Sol}	Self-cal solution noise per visibility required for convergence
σ_{Cfn}	Source confusion noise
σ_{Cal}	"External" gain calibration noise
σ_T	Thermal noise
σ_N	Nighttime far sidelobe noise term
σ_D	Daytime (includes Sun) far sidelobe noise term
σ_S	Near-in sidelobe noise term
σ_P	Main beam slow pointing induced noise term
σ'_P	Main beam rapid pointing induced noise term
σ_Q	Main beam asymmetry induced noise term
σ_B	Main beam frequency modulation induced noise term
σ_M	Source modelling error induced noise term

We summarise the key parameter definitions from RD3 in Table 1 for convenience. Each of the effects considered is described by a parametric model, together with a parameterised estimate of what constitutes an independent time and frequency interval for the effect in question. These equations are used to estimate the "noise-like" modulations that are introduced into the visibilities and subsequently into images. Effects that pertain to sources within the imaged field of view lead to a straightforward increase to the noise floor in the image. Effects that pertain to sources outside of the imaged field of view increase the image noise floor less directly. They do so by two distinct mechanisms. The first is via the instantaneous sidelobes of the point spread function. The second is via the decreased precision of the self-calibration solutions that lead to enhanced noise-like fluctuations from sources within the imaged field. Both of these indirect mechanisms are suppressed by the number, N, of dishes/stations within the array, since this improves the instantaneous PSF as N^{-2}, as well as the self-cal noise propagation as $N^{-1.5}$ (equation 17 of RD3). The smaller exponent of the self-cal noise term (-1.5 versus -2) means that this effect will dominate over the sidelobe noise term under most circumstances. For the current generation of arrays with N ≈ 30, the self-cal propagation noise has a similar magnitude for sources both inside and outside the imaged field. For large N arrays, there is substantial suppression of the noise due to out-of-field sources.

4 Application of error budget analysis

We apply the parametric analysis of error terms as outlined in RD3 to the most relevant current facilities and subsequently to the SKA1 deployment below. The specific current facilities discussed for comparison will be the B-configuration of the recently upgraded VLA to provide some context for SKA1-Mid and the NL-based High Band Antenna (HBA) deployment of LOFAR for SKA1-Low. The assumed instrumental parameters (as defined in RD3) are summarised in Table 2. It should be noted that the analysis is being applied **in all cases to a single polarisation product**.

Table 2. Assumed instrumental parameters of comparison and SKA1 arrays.

Telescope	VLA B-Cfg	SKA1-Mid	LOFAR-NL	SKA1-Low
N	27	197	62	512
d (m)	25	15	31	35
B_{Max} (km)	11	150	80	65
B_{Med} (km)	3.5	2.6	6.6	4.0
φ_C	0.1	0.1	0.2	0.2
τ_C (min)	15	15	15	15
η_F	0.1	0.2	0.5	0.5
ε_S	0.02	0.01	0.1	0.1
P (arcs)	10	10		
τ_P (min)	15	15		
ε'_P	0.01	0.01	0.01	0.01
τ'_P (sec)	5	5	60	60
ε_Q	0.055	0.04	0.01	0.01
ε_B	0.05	0.01	0.01	0.01
l_C (m)	8.2	7	10	10

4.1 VLA B-Configuration

The B-configuration of the VLA has the 27 VLA dishes of 25m diameter distributed to have a maximum baseline, B_{Max} = 11km, and a median baseline of B_{Med} = 3.5km as shown in Figure 1 for an 8-hour tracked observation at a declination, δ = +30°.

The other instrumental quantities that are likely to influence the imaging performance are tabulated in Table 2 and have been defined and discussed at some length in RD3. Specifically: the far side-lobe scaling factor η_F; the near-in side-lobe amplitude ε_S; the slowly varying (systematic) pointing error P, in arcseconds, and its variability timescale τ_P, in minutes; the more rapidly varying (random) pointing error fractional amplitude on the main beam flank ε'_P (= P_{rad} d / λ), and its variability timescale τ'_P, in seconds; the amplitude of polarisation beam squint or squash ε_Q; the amplitude of frequency modulation of the beam ε_B, and the characteristic equivalent cavity dimension for this modulation l_C, in meters. We depart slightly from the definitions given in RD3 to allow for two distinct classes – systematic and random – of pointing error that will apply to dishes.

The noise error budget on the self-cal solution timescale is depicted in Figure 2. Achieving a thermal noise level, $\sigma_T < \sigma_{Sol}$, that permits a useful self-cal solution to be obtained (with error less than 0.5 rad) using the signal from sources that occur in a random field requires substantial time and frequency averaging by about a factor of 10 over the values of (τ*, $\Delta\nu$*) that would limit time and frequency smearing effects to be less than 10% of the point spread function (PSF) at the edge of the main beam. Typical averaging times of about τ_{Sol} = 30 seconds and relative bandwidths $\Delta\nu_{Sol}/\nu = 2 \times 10^{-3}$ are needed. The implication is that special measures will be needed to circumvent or account for smearing effects in the source modelling and calibration strategy. Since none of the other error terms considered exceed the thermal noise on this timescale it is anticipated that self-cal can be successfully applied to observations of this type.

4.1.1 Deep Spectral Line Observations with the VLA

The noise error budget for a deep spectral line ($\Delta\nu_T/\nu = 1 \times 10^{-3}$, where $\Delta\nu_T$ is the bandwidth) observation, in which 100 repeats of a 10 hour track are obtained, is depicted in Figure 3. For this calculation it is assumed that all systematic error terms, i.e. those that relate to specific errors in the model of the sky or the stationary instrumental response, do not diminish when averaging multiple tracks. Only the partial cancellation due to averaging within an individual track diminishes the amplitude of errors of this type. Since the thermal noise is less than the noise level expected after external calibration of the field, $\sigma_T < \sigma_{Cal}$, below 2 GHz it is clear that self-cal will be necessary to achieve the required dynamic range in a random pointing direction. Impediments to achieving thermal noise limited imaging at these depths become more pronounced as the observing frequency declines. The three variants of the curve labelled σ_M pertain to three different assumptions about the source modelling precision that is achieved for sources in the field, namely ε_M = 0.1, 0.01 and 0.001. As discussed in RD3, achievement of ε_M = 0.01 is challenging, but realistic with current source modelling methods if time and bandwidth smearing effects are explicitly taken into account. The instrumental parameters that would suppress all error terms to values below the thermal noise curve are listed in Table 3. These are designated with the same parameter names as used previously but are distinguished by underlining. Those instances where the requirement is less extreme than the value assumed in Table 2 are highlighted in green, those where the requirement must be improved by more than an order of magnitude are highlighted in red, while those that exceed the assumed value by a factor in the range of 1 – 10 are highlighted in yellow.

Since the instrumental parameters themselves can often not be modified, the requirements In Table 3 can be interpreted as the levels down to which residual effects of the type under consideration must be calibrated in order not to represent a performance limitation. What this implies in practise for this example is:

- Post-calibration frequency modulation of the main beam gain must be less than $\underline{\varepsilon_B}$ = 0.006.
- Post-calibration residual main beam azimuthal asymmetries must be less than $\underline{\varepsilon_Q}$ = 0.01.
- Long-duration systematic pointing offsets must be reduced to below P = 8 arcsec.
- The brightest 0.7 dex [= $\log_{10}(\varepsilon_S/\underline{\varepsilon_S})$ = $\log_{10}(0.02/0.004)$] of random sources occurring within the main beam near-in sidelobes must be included in the self-cal model.

4.1.2 Deep Continuum Observations with the VLA

The case of a similarly deep broad-band ($\Delta\nu_T/\nu$ = 0.3) continuum observation is depicted in Figure 3. In this case, many more issues can constitute a performance limitation. As for the spectral line case, the lowest observing frequencies are found to be most challenging. The required parameters to suppress each noise term below the thermal noise are listed in Table 3. Many more parameters require significant suppression beyond what is assumed to be provided by the instrument itself. For this example:

- A very high modelling precision of $\underline{\varepsilon_M}$ =0.002 must be achieved.
- Post-calibration frequency modulation of the main beam gain must be less than $\underline{\varepsilon_B}$ = 0.003.
- Post-calibration residual main beam azimuthal asymmetries must be less than $\underline{\varepsilon_Q}$ = 0.0007.
- Random short time-constant pointing variations must be kept below $\underline{\varepsilon'_P}$ = 0.002 (about 3 arcseconds at GHz frequencies).
- Post-calibration long-duration systematic pointing offsets must be reduced to P = 0.6 arcsec.
- The brightest 1.3 dex [= $\log_{10}(\varepsilon_S/\underline{\varepsilon_S})$ = $\log_{10}(0.02/0.001)$] of random sources occurring within the main beam near-in sidelobes must be included in the self-cal model.

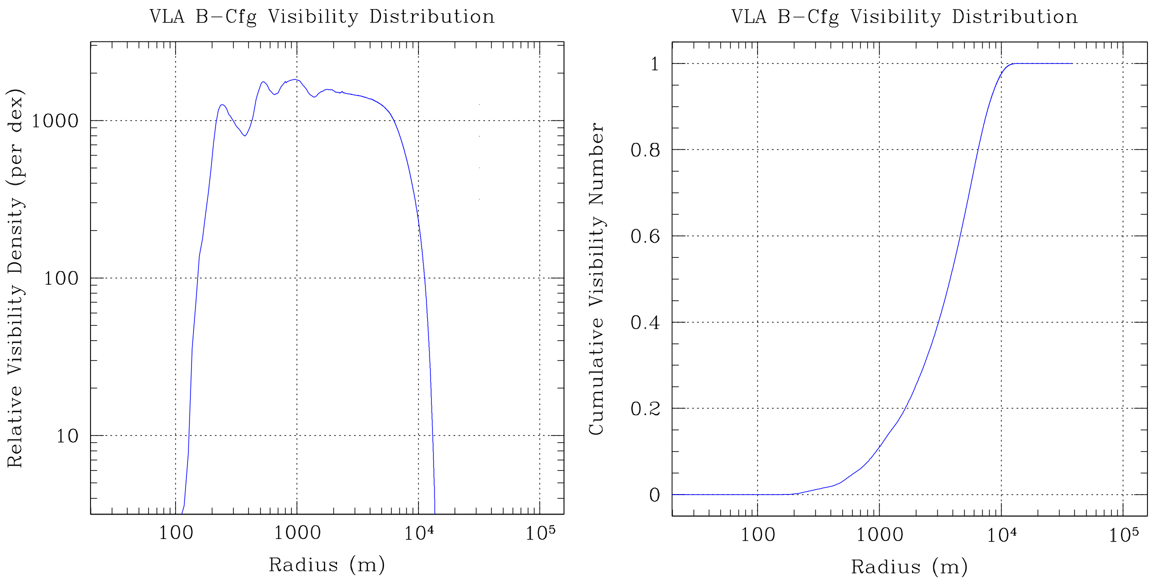

Figure 1. Relative visibility density (left) and cumulative visibility distribution (right) for the VLA B-configuration based on an 8-hour track at δ = +30°. The median baseline length for such an observation is 3.5km.

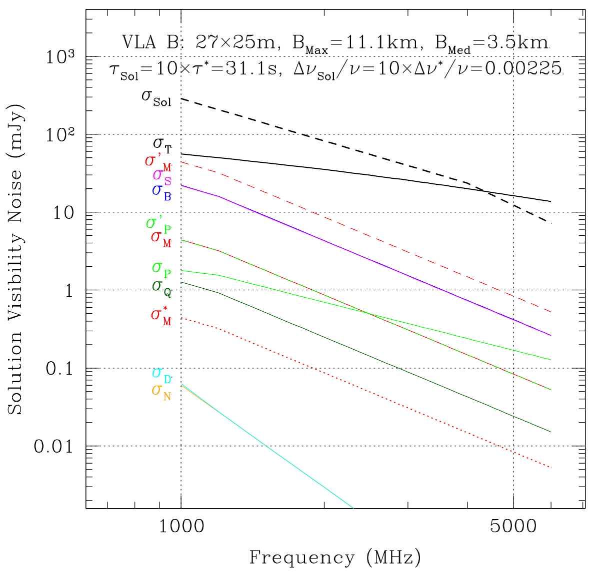

Figure 2. Noise error budget on the self-cal solution timescale for the VLA B-configuration as function of observing frequency. The various error terms are colour coded and individually plotted.

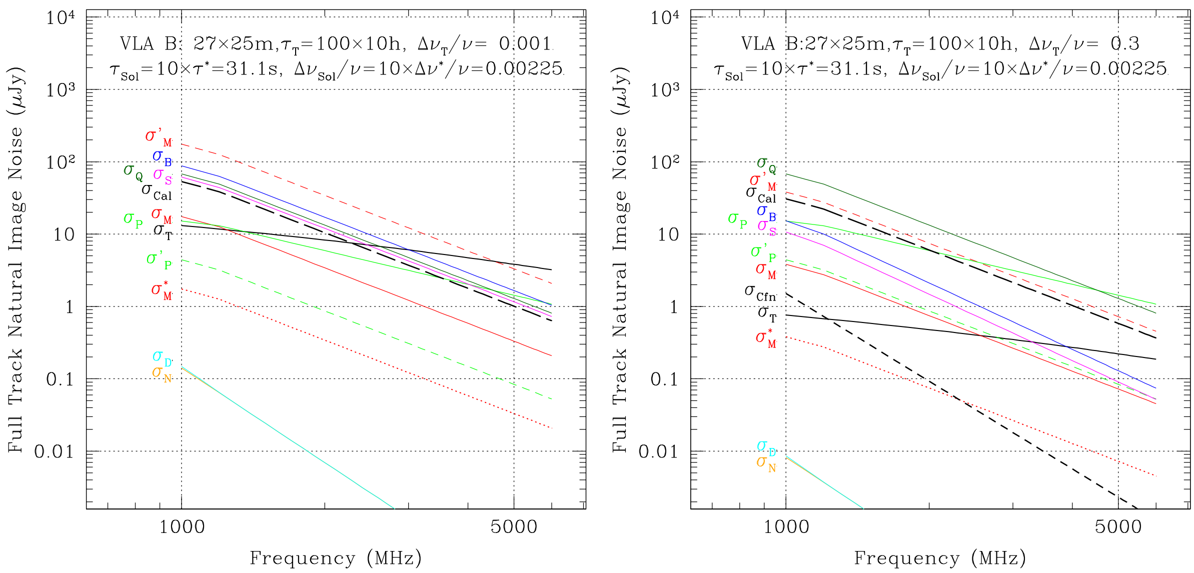

Figure 3. Noise error budget for a deep spectral line (left) and broad-band continuum (right) observation with the VLA B-configuration as function of observing frequency. The various error terms are colour coded and individually plotted.

Table 3. Required instrumental/calibration parameters to achieve thermal noise limited performance.

Telescope | Application	η_F	ε_S	P	ε'_P	ε_Q	ε_B	ε_M
VLA B-Cfg | Self-cal Sol	-	-	-	-	-	-	0.1
| Spectral	-	0.004	8	0.03	0.01	0.006	0.01
| Continuum	-	0.001	0.6	0.002	0.0007	0.003	0.002
SKA1-Mid | Self-cal Sol	-	-	-	-	-	-	-
| Spectral	-	0.002	8	0.1	0.003	0.003	0.003
| Continuum	-	0.0006	1	0.01	0.0003	0.001	0.001
LOFAR-NL | Self-cal Sol	-	-	-	-	-	-	0.1
| Spectral	0.3	0.001	-	0.03	0.003	0.002	0.002
| Continuum	0.3	0.001	-	0.006	0.0005	0.02	0.002
SKA1-Low | Self-cal Sol	0.15	-	-	-	-	-	0.1
| Spectral	0.05	0.0005	-	0.02	0.003	0.002	0.001
| Continuum	0.08	0.0006	-	0.004	0.0004	0.01	0.001

4.2 SKA1-Mid

The current Baseline Design [RD2] calls for the deployment of 133 SKA dishes of 15m diameter to be used in conjunction with the 64 MeerKAT dishes of 13.5m diameter. The 197 dishes will be deployed in a centrally condensed configuration that has a maximum baseline, B_{Max} = 150km, and a median baseline of B_{Med} = 2.6km as shown in Figure 4 for an 8-hour tracked observation at a declination, δ = –30°.

Although there is still some uncertainty relating to the feed systems that will be available on the MeerKAT dishes as well as their performance, we will begin by making the simplifying assumption that all 197 dishes of SKA1-Mid have comparable frequency coverage and performance.

The noise error budget on the self-cal solution timescale is depicted in Figure 5. Achieving a thermal noise level, $\sigma_T < \sigma_{Sol}$, that permits a useful self-cal solution to be obtained (with error less than 0.5 rad) using the signal from sources that occur in a random field requires substantial time and frequency averaging by about a factor of 10 over the values of (τ^*, $\Delta\nu^*$) that would limit time and frequency smearing effects to be less than 10% of the point spread function (PSF) at the edge of the main beam. Typical averaging times of about τ_{Sol} = 1.4 seconds and relative bandwidths $\Delta\nu_{Sol}/\nu = 1 \times 10^{-4}$ are needed. The implication is that special measures will be needed to circumvent or account for smearing effects in the source modelling and calibration strategy. Since none of the other error terms considered exceed the thermal noise on this timescale it is anticipated that self-cal can be successfully applied to observations of this type.

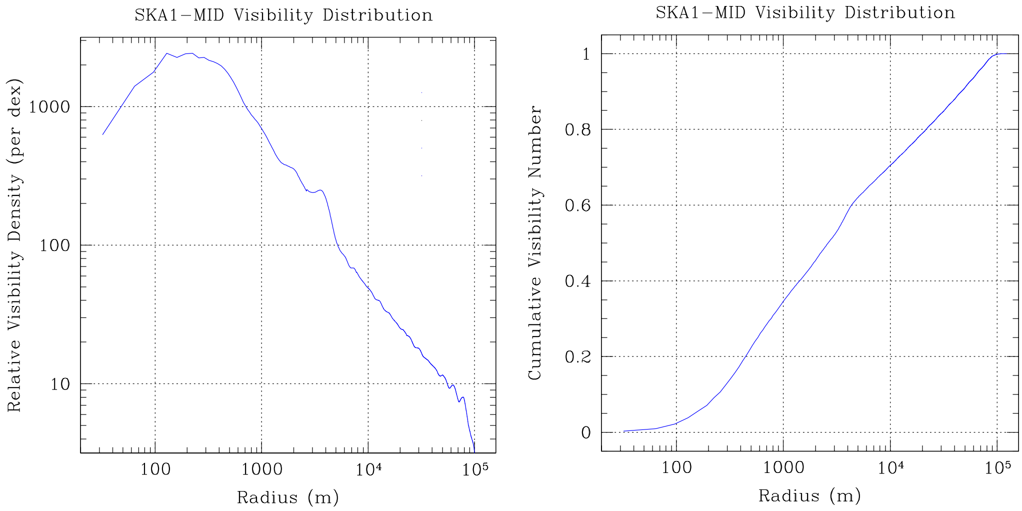

Figure 4. Relative visibility density (left) and cumulative visibility distribution (right) for SKA1-Mid based on an 8-hour track at δ = -30°. The median baseline length for such an observation is 2.6km.

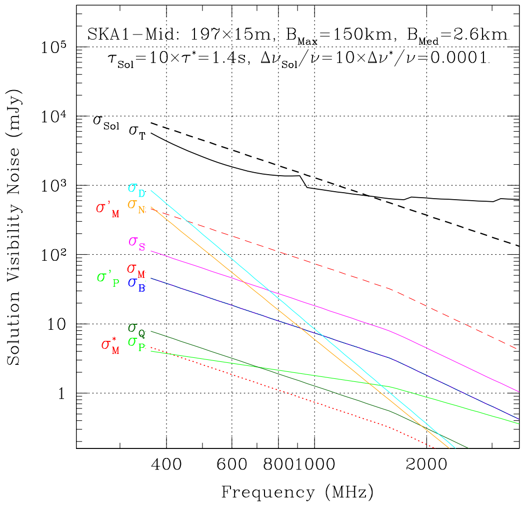

Figure 5. Noise error budget on the self-cal solution timescale for SKA1-Mid as function of observing frequency. The various error terms are colour coded and individually plotted.

4.2.1 Deep Spectral Line Observations with SKA1-Mid

The noise error budget for a deep spectral line ($\Delta\nu_T/\nu = 1 \times 10^{-3}$) observation, in which 100 repeats of a 10 hour track are obtained, is depicted in Figure 6. As noted previously, it is assumed that all systematic error terms, ie. those that relate to specific errors in the model of the sky or the stationary instrumental response, do not diminish when averaging multiple tracks. Only the partial cancellation due to averaging within an individual track diminishes the amplitude of errors of this type. Since the thermal noise is much less than the noise level expected after external calibration of the field, $\sigma_T << \sigma_{Cal}$, it is clear that self-cal will be necessary to achieve the required dynamic range in a random pointing direction. Impediments to achieving thermal noise limited imaging at these depths become more pronounced as the observing frequency declines, although the majority of effects apply to all frequencies below about 1.8 GHz with a similar magnitude.

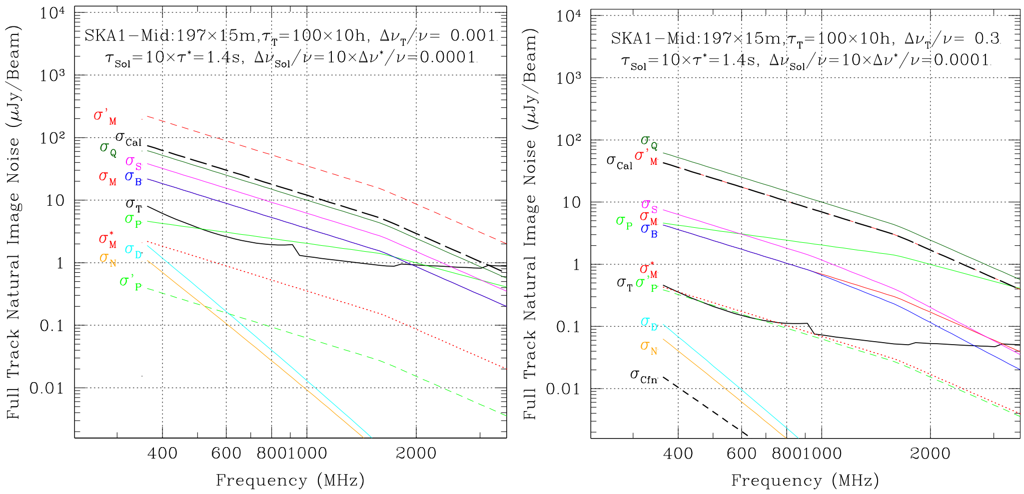

Figure 6. Noise error budget for a deep spectral line (left) and broad-band continuum (right) observation with SKA1-Mid as function of observing frequency. The various error terms are colour coded and individually plotted.

For this example:

- An very high modelling precision of $\underline{\varepsilon}_M$ =0.003 must be achieved.
- Post-calibration frequency modulation of the main beam gain must be less than $\underline{\varepsilon}_B$ = 0.003.
- Post-calibration residual main beam azimuthal asymmetries must be less than $\underline{\varepsilon}_Q$ = 0.003.
- Post-calibration long-duration systematic pointing offsets must be reduced to P = 8 arcsec.
- The brightest 0.7 dex [= $\log_{10}(\varepsilon_S/\underline{\varepsilon}_S)$ = $\log_{10}(0.01/0.002)$] of random sources occurring within the main beam near-in sidelobes must be included in the self-cal model.

4.2.2 Deep Continuum Observations with SKA1-Mid

The case of a similarly deep broad-band ($\Delta\nu_T/\nu = 0.3$) continuum observation in depicted in Figure 6. For this example:

- An extremely high modelling precision of $\underline{\varepsilon}_M$ =0.001 must be achieved.
- Post-calibration frequency modulation of the main beam gain must be less than $\underline{\varepsilon}_B$ = 0.001.
- Post-calibration residual main beam azimuthal asymmetries must be less than $\underline{\varepsilon}_Q$ = 0.0003.
- Post-calibration long-duration systematic pointing offsets must be reduced to P = 1 arcsec.
- The brightest 1.2 dex [= $\log_{10}(\varepsilon_S/\underline{\varepsilon}_S)$ = $\log_{10}(0.01/0.0006)$] of random sources occurring within the main beam near-in sidelobes must be included in the self-cal model.

4.3 LOFAR-NL

The LOFAR High Band Antenna (HBA) facility operating between 120 – 245 MHz, currently consists of 62 stations within the Netherlands, including 48 stations within a core region of about 5km diameter that are deployed as close pairs and an additional 14 "remote" stations that are located at distances of up to about 55km. Although the remote stations have a larger physical size than those in the core due to the fact that they have twice the number of antennas, it has been found that the "lowest common station size" approach, where all stations are effectively 31m in diameter, is the most effective station beam-forming strategy in practise. LOFAR also includes a Low Band Antenna (LBA) system that operates between about 30 – 80 MHz, but we will restrict our comparison to only the HBA system.

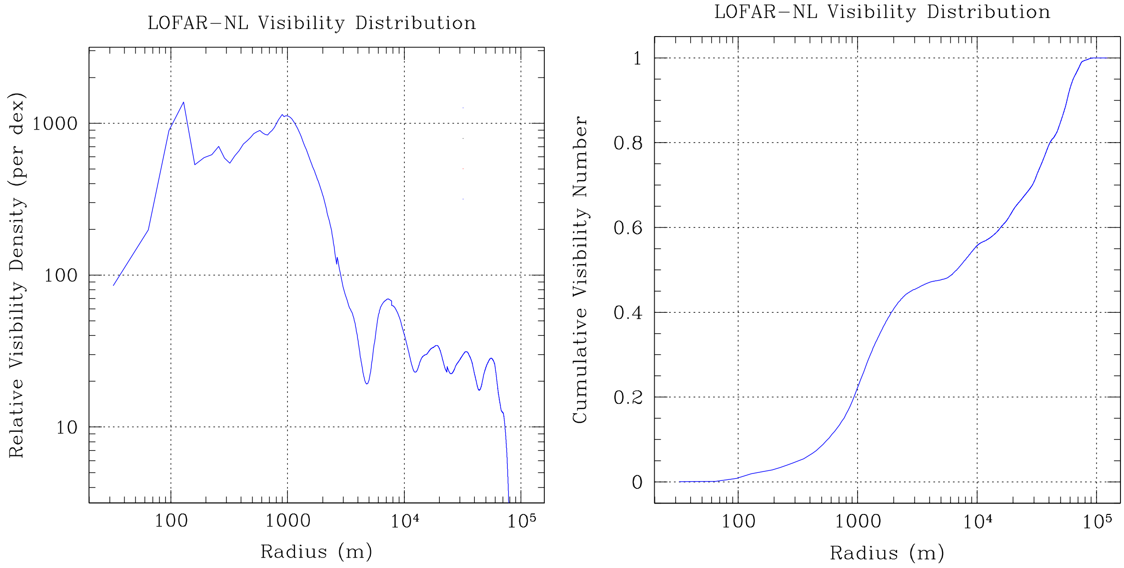

Figure 7. Relative visibility density (left) and cumulative visibility distribution (right) for LOFAR-NL based on a 4-hour track at δ = +30°. The median baseline length for such an observation is 6.6km.

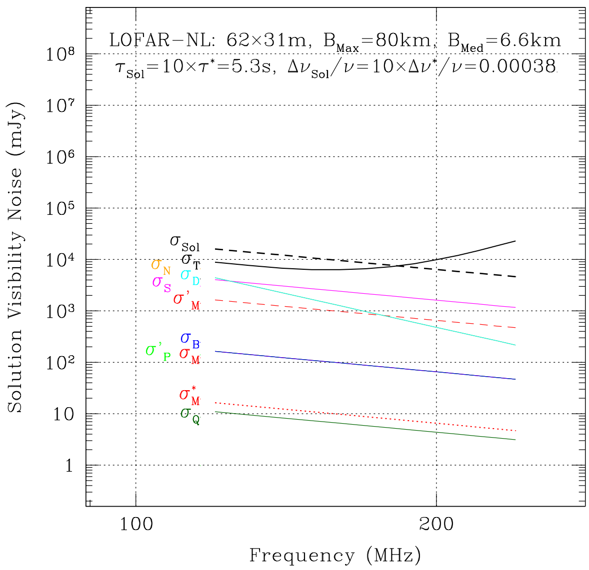

Figure 8. Noise error budget on the self-cal solution timescale for LOFAR-NL HBA as function of observing frequency. The various error terms are colour coded and individually plotted.

The noise error budget on the self-cal solution timescale is depicted in Figure 8. Achieving a thermal noise level, $\sigma_T < \sigma_{Sol}$, that permits a useful self-cal solution to be obtained (with error less than 0.5 rad) using the signal from sources that occur in a random field requires substantial time and frequency averaging by about a factor of 10 over the values of (τ^*, $\Delta\nu^*$) that would limit time and frequency smearing effects to be less than 10% of the point spread function (PSF) at the edge of the main beam. Typical averaging times of about τ_{Sol} = 5.3 seconds and relative bandwidths $\Delta\nu_{Sol}/\nu = 4 \times 10^{-4}$ are needed. The implication is that special measures will be needed to circumvent or account for smearing effects in the source modelling and calibration strategy. It should be noted that we extend the approach outlined in RD3 by utilising the ε_B and l_C parameters tabulated in Table 2 and σ_B plotted in the Figures to represent a residual frequency modulation of the aperture array station gain with frequency that is comparable to the "standing wave" phenomenon seen in dishes. The value of l_C = 10m represents a 15 MHz assumed periodicity for such an effect for the purposes of illustration.
Since none of the other error terms considered exceed the thermal noise on this timescale it is anticipated that self-cal can be successfully applied to observations of this type.

4.3.1 Deep Spectral Line Observations with LOFAR

The noise error budget for a deep spectral line ($\Delta\nu_T/\nu = 1 \times 10^{-2}$) observation, in which 100 repeats of a 4 hour track are obtained, is depicted in Figure 9. As noted previously, it is assumed that all systematic error terms, ie. those that relate to specific errors in the model of the sky or the stationary instrumental response, do not diminish when averaging multiple tracks. Only the partial cancellation due to averaging within an individual track diminishes the amplitude of errors of this type. Since the thermal noise is much less than the noise level expected after external calibration of the field, $\sigma_T << \sigma_{Cal}$, it is clear that self-cal will be necessary to achieve the required dynamic range in a random pointing direction. Impediments to achieving thermal noise limited imaging at these depths become more pronounced as the observing frequency declines.

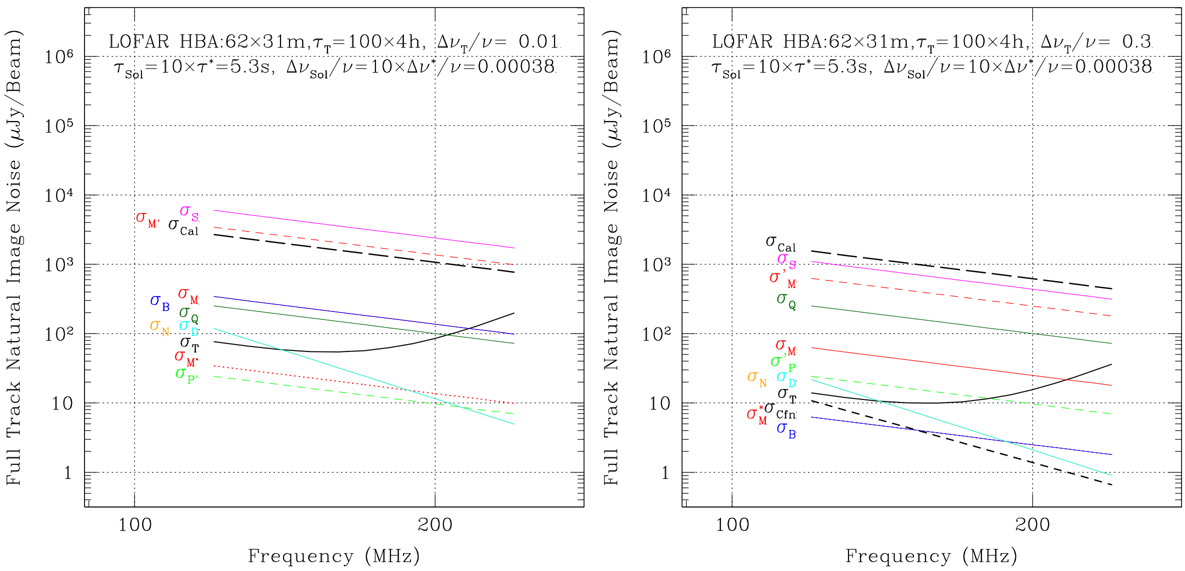

Figure 9. Noise error budget for a deep spectral line (left) and broad-band continuum (right) observation with LOFAR-NL as function of observing frequency. The various error terms are colour coded and individually plotted.

For this example:

- A very high modelling precision of ε_M =0.002 must be achieved.

- Post-calibration frequency modulation of the main beam gain must be less than $\underline{\varepsilon}_B$ = 0.002.
- Post-calibration residual main beam azimuthal asymmetries must be less than $\underline{\varepsilon}_Q$ = 0.003.
- The brightest 2.0 dex [= $\log_{10}(\varepsilon_S/\underline{\varepsilon}_S)$ = $\log_{10}(0.1/0.001)$] of random sources occurring within the main beam near-in sidelobes must be included in the self-cal model.
- The brightest 0.2 dex [= $\log_{10}(\eta_F/\underline{\eta}_F)$ = $\log_{10}(0.5/0.3)$] of sources occurring over the entire visible sky must be included in the self-cal model and subtracted.

4.3.2 Deep Continuum Observations with LOFAR

The case of a similarly deep broad-band ($\Delta\nu_T/\nu$ = 0.3) continuum observation in depicted in Figure 9. For this example:

- A very high modelling precision of $\underline{\varepsilon}_M$ =0.002 must be achieved.
- Post-calibration residual main beam azimuthal asymmetries must be less than $\underline{\varepsilon}_Q$ = 0.0005.
- Random electronic gain variations that induce station "pointing" offsets must be kept below $\underline{\varepsilon}'_P$ = 0.006.
- The brightest 1.0 dex [= $\log_{10}(\varepsilon_S/\underline{\varepsilon}_S)$ = $\log_{10}(0.01/0.001)$] of random sources occurring within the main beam near-in sidelobes must be included in the self-cal model.
- The brightest 0.2 dex [= $\log_{10}(\eta_F/\underline{\eta}_F)$ = $\log_{10}(0.5/0.3)$] of sources occurring over the entire visible sky must be included in the self-cal model and subtracted.

4.4 SKA1-Low

The current Baseline Design [RD2] calls for the deployment of about 131000 log periodic antennas. While the detailed deployment strategy at station level is still being assessed, a good working assumption will be deployment of a total of about 512 stations of 35m diameter. The stations will be deployed in a centrally condensed configuration that has a maximum baseline, B_{Max} = 65km, and a median baseline of B_{Med} = 4.0km as shown in Figure 10 for a 4-hour tracked observation at a declination, δ = –30°.

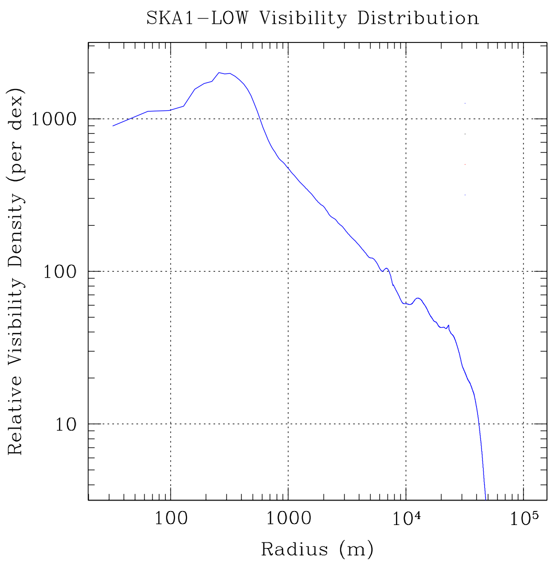

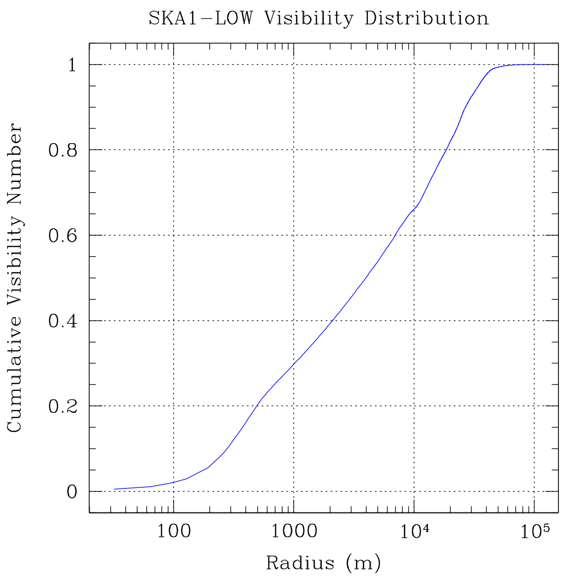

Figure 10. Relative visibility density (left) and cumulative visibility distribution (right) for SKA1-Low based on a 4-hour track at δ = -30°. The median baseline length for such an observation is 4.0km.

The noise error budget on the self-cal solution timescale is depicted in Figure 11. Achieving a thermal noise level, $\sigma_T < \sigma_{Sol}$, that permits a useful self-cal solution to be obtained (with error less than 0.5 rad) using the signal from sources that occur in a random field requires substantial time and frequency averaging by about a factor of 10 over the values of (τ^*, $\Delta\nu^*$) that would limit time and frequency smearing effects to be less than 10% of the point spread function (PSF) at the edge of the main beam. Typical averaging times of about τ_{Sol} = 7.4 seconds and relative bandwidths $\Delta\nu_{Sol}/\nu = 5 \times 10^{-3}$ are needed. The implication is that special measures will be needed to circumvent or account for smearing effects in the source modelling and calibration strategy.

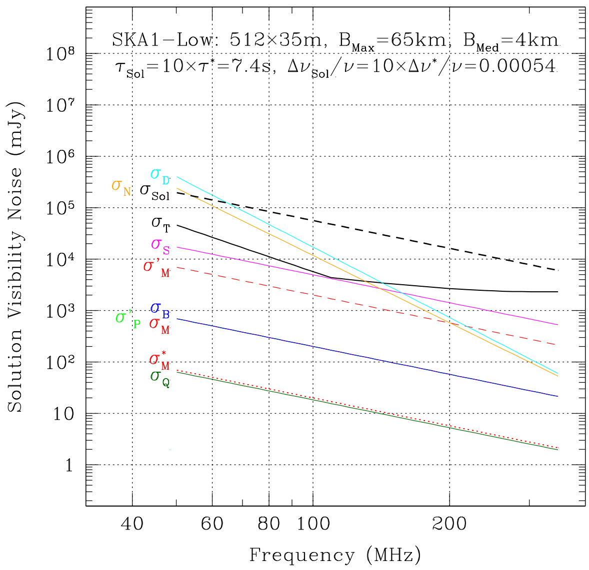

Figure 11. Noise error budget on the self-cal solution timescale for SKA1-Low as function of observing frequency. The various error terms are colour coded and individually plotted.

Unlike all of the previous cases considered in this memo, there are likely to be significant complications to self-calibration at frequencies below about 120 MHz due to far side-lobe pick-up of all sources on the sky. A moderate degree of “all-sky self-cal” (explicit modelling of the apparent instrumental response to widely distributed sources on the sky) will be necessary from the outset to enable successful calibration to proceed. The effective 1.4 GHz “noise” due to 2π sr of the extragalactic sky is shown in Figure 4 of RD3. The median baseline length of SKA1-Low B_{Med} = 4.0km observing near 140 MHz corresponds to an equivalent 1.4GHz baseline length ($B'_{Med} = B_{Med} (\nu/1.4\mathrm{GHz})^{-1}$) of about 0.40km. For 1.4 GHz equivalent baselines below B'_{Med} = 2km it is the Sun that dominates the sky noise. Sensitive observations in this regime will require night-time observing. On these baselines the brightest dex of night-time sky noise is due to the highest flux density bin ($S_{1.4}$ > 30 Jy) of discrete sources; the so-called “A-team”. While few in number density (2.4 sr^{-1}) these NVSS source components have a maximum 1.4 GHz flux density of 860 Jy, a median “size” of 160 arcsec and spectral index α = -0.8. For a random pointing direction we can expect about 15 of such sources above the horizon at any time. Rather than being conveniently “point-like” these source components instead have complex morphologies that will require detailed individual modelling. In fact, the two brightest Northern hemisphere sources, Cygnus A (α,δ = 20^h,+41°) and Cas A (α,δ = 23^h.5,+59°), together account for all source components with $S_{1.4}$ > 340 Jy. These are followed by a handful of more uniformly distributed sources exceeding $S_{1.4}$ > 100 Jy. The latitude of the SKA1-Low site (-27° South) implies that the two brightest sources will only occasionally be above the horizon.

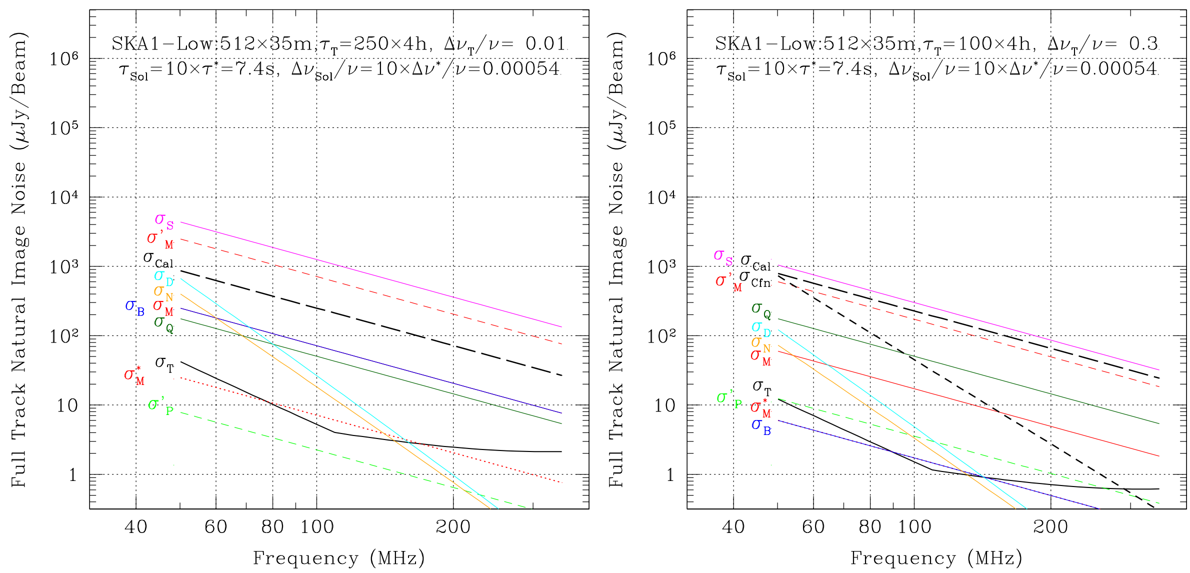

Figure 12. Noise error budget for a deep spectral line (left) and broad-band continuum (right) observation with SKA1-Low as function of observing frequency. The various error terms are colour coded and individually plotted.

4.4.1 Deep Spectral Line Observations with SKA1-Low

The noise error budget for a deep spectral line ($\Delta\nu_T/\nu = 1 \times 10^{-2}$) observation, in which 250 repeats of a 4 hour track are obtained, is depicted in Figure 12. As noted previously, it is assumed that all systematic error terms, i.e. those that relate to specific errors in the model of the sky or the stationary instrumental response, do not diminish when averaging multiple tracks. Only the partial cancellation due to averaging within an individual track diminishes the amplitude of errors of this type. Since the thermal noise is much less than the noise level expected after external calibration of the field, $\sigma_T \ll \sigma_{Cal}$, it is clear that self-cal will be necessary to achieve the required dynamic range in a random pointing direction. Impediments to achieving thermal noise limited imaging at these depths are most pronounced between about 100 and 150 MHz, where the sensitivity is highest.

For this example:

- An extremely high modelling precision of $\underline{\varepsilon}_M$ =0.001 must be achieved.
- Post-calibration frequency modulation of the main beam gain must be less than $\underline{\varepsilon}_B$ = 0.002.
- Post-calibration residual main beam azimuthal asymmetries must be less than $\underline{\varepsilon}_Q$ = 0.003.
- The brightest 2.3 dex [= $\log_{10}(\varepsilon_S/\underline{\varepsilon}_S)$ = $\log_{10}(0.1/0.0005)$] of random sources occurring within the main beam near-in sidelobes must be included in the self-cal model.
- The brightest 1.0 dex [= $\log_{10}(\eta_F/\underline{\eta}_F)$ = $\log_{10}(0.5/0.05)$] of sources occurring over the entire visible sky must be included in the self-cal model and subtracted.

4.4.2 Deep Continuum Observations with SKA1-Low

The case of a similarly deep broad-band ($\Delta\nu_T/\nu = 0.3$) continuum observation in depicted in Figure 12. In this case it should ne noted that natural source confusion, σ_{Cfn}, will prove a limitation to the depth that can be achieved in Stokes I images below about 300 MHz. However, leaving this aside one would otherwise require:

- An extremely high modelling precision of $\underline{\varepsilon}_M$ =0.001 must be achieved.

- Post-calibration residual main beam azimuthal asymmetries must be less than $\underline{\varepsilon}_Q$ = 0.0004.
- Random electronic gain variations that induce station "pointing" offsets must be kept below $\underline{\varepsilon'}_P$ = 0.004.
- The brightest 1.2 dex [= $\log_{10}(\varepsilon_S/\underline{\varepsilon}_S)$ = $\log_{10}(0.01/0.0006)$] of random sources occurring within the main beam near-in sidelobes must be included in the self-cal model.
- The brightest 0.8 dex [= $\log_{10}(\eta_F/\underline{\eta}_F)$ = $\log_{10}(0.5/0.08)$] of sources occurring over the entire visible sky must be included in the self-cal model and subtracted.

5 Implications

The analysis of Section 4 provides constraints on some of the requirements that must jointly be provided by (a) the instrument design and (b) the calibration strategy to enable deep integrations to achieve thermal noise limited performance. Those *joint* requirements are expressed by the values in Table 3. For some parameters, the entire requirement could in principle be provided by the instrument design. In those cases no further improvement would need to be provided by the method of calibration. In practise, only a portion of each requirement is typically realised by the most cost-effective instrumental design. The remainder can be most plausibly implemented within the calibration strategy. Historically, many facilities have begun with only the limited performance enabled by the intrinsic properties of the instrument and the most basic calibration methods. Over time, enhanced performance has been realised via the development of more advanced calibration algorithms and greatly improved computing capacity. It is very likely that a similar situation will apply to the SKA deployment. The current situation only differs from previous ones in that a crude indication of the magnitude of many potential impediments has been quantified in advance. This should provide a basis for guiding design decisions in both the hardware and software.

5.1 VLA B-Configuration

The VLA has not yet been used extensively to obtain deep observations, despite being in operation since 1980. Some of the deepest published observations are those of RD4, where 50 hours of net integration were obtained in the B-configuration at 1190 – 1426 MHz. These data reached a depth of 85 µJy/beam by averaging two polarisations at a spectral resolution of $\Delta\nu/\nu = 1 \times 10^{-4}$, in those portions of the spectrum that were not severely degraded by RFI. Comparison with Figure 3 is not entirely appropriate given the different spectral resolution and total depth involved, however Figure 3 does suggest that only towards the bottom of the observed band would the strongest systematic errors begin to approach a thermal noise floor of ($\sqrt{2}$ ×) 85 µJy. The prediction is that deeper integrations of this type would need to take explicit account of polarisation beam squint, frequency modulation of the beam shape and continuum sources in the sidelobes of the main beam. Another relevant comparison is with the observations reported in RD5, where a total of 140 hours where obtained, although primarily in the more extended A-configuration (B_{Max} = 36.4km). Those observations near 1400 MHz had $\Delta\nu/\nu = 0.03$ and achieved a depth of 2.7 µJy/beam by averaging two polarisations. As noted by the authors (in Section 3.2), they found it necessary to develop a self-cal model for the field based on a multi-facet imaging strategy (to minimise both smearing and w-projection effects in the model for the field) and ultimately to process each frequency band, each polarisation and each hour angle range of the tracking coverage with its own self-calibration model in order to reach their final depth. These are precisely the performance limiting effects predicted to be of most relevance in the analysis of Section 4.1.

5.2 SKA1-Mid

Exquisite knowledge of the frequency resolved beam shape in each polarisation product together with its variation with time will be vital to achieving thermal noise limited imaging performance in deep integrations. Residual azimuthal asymmetries of a systematic nature must be kept below, $\varepsilon_Q = 0.0003$ and residual systematic frequency modulations below, $\varepsilon_B = 0.001$. Measures will need to be adopted to provide very high temporal stability of the beam and a high precision model must be developed, calibrated and applied throughout the imaging and self-calibration process.
Mechanical, slowly varying pointing errors of systematic origin must be kept below about P = 1 arcsec, which will be a significant challenge. There is much less sensitivity to rapidly varying pointing errors that are intrinsically random, which could be as large as, $\varepsilon'_P = 0.01$ (where $\varepsilon'_P = P'_{rad}\ d / \lambda$ yielding $P' \approx$ 15 arcseconds at GHz frequencies) before becoming a limitation.

Extremely high source modelling precision, $\varepsilon_M = 0.001$, must be routinely achieved. This will likely require development of advanced source representation strategies (rather than simply Gaussians or CLEAN components), together with wide-field self-cal and imaging methods that minimise time and frequency smearing effects as well as w-projection distortions. Although the "forward" problem, of calculating a wide-field image that is free of these distortions, is relatively straightforward, the "reverse" problem, of adequately constraining the self-cal solutions that are, for signal-to-noise reasons, averaged over much longer time and frequency intervals than appropriate for large off-axis distances, may necessitate a multi-faceted processing of the visibilities.

The self-cal model will need to include a sufficient population of sources occurring within the first sidelobe of the beam to reduce the effective residual response to $\underline{\varepsilon_S} = 0.0006$. To put this in context, at 1 GHz, the brightest random source within the first sidelobe (with total area of about 4.6 deg^2) will have an intrinsic flux density of about $S_{Max} = 660$ mJy. All sources within the first sidelobe down to an apparent flux density of $\underline{S_{Min}} = S_{Max} \times \underline{\varepsilon_S} = 0.4$ mJy will then need to be included in the self-cal model. In the event that an actual peak sidelobe response of $\varepsilon_S = 0.01$ is achieved with the specific dish and feed design, then this corresponds to 20 or so sources with intrinsic flux density exceeding about 40 mJy in this area. In the event that a higher peak sidelobe level, of say $\varepsilon_S = 0.05$, were achieved, then the same constraint would correspond to the 100 or so sources with intrinsic flux density greater than about 8 mJy.

5.3 LOFAR-NL

One of the primary scientific goals of the LOFAR facility is statistical detection of the HI brightness fluctuations associated with the Epoch of Reionisation at frequencies between about 120 and 200 MHz. This will require very high sensitivity to angular scales of some 10's of arcmin as well as an exquisite ability to subtract the very bright foreground source populations. The array configuration (shown in Figure 7) addresses this goal with essentially an equal split of the collecting area between a core region of a few km in extent and the more extended array. The median overall baseline length (which will play a dominant role in determining the signal to noise ratio during the calibration process) is a relatively large $B_{Med} = 6.6$km. This is a major simplifying factor as the impediments to successful calibration increase dramatically as the baseline length declines.
Several years of LOFAR data acquisition have allowed some of the calibration challenges at these low frequencies to be addressed. The deepest high-resolution continuum observations of the North Celestial Pole region published to date in RD6 have reached a depth of 100 μJy/beam in an 18 hour integration. Unpublished reports suggest that the same team have reached 25 μJy/beam after 170 hours of integration. The calibration strategy employed for deep imaging relies from the outset on modelling the instrumental response to the brightest discrete sources above the horizon at any time.

As noted previously, current experience is limited to consideration of only two of such "all-sky self-cal" sources. These sources are included in the direction dependent self-calibration of the main station beam and its near-in sidelobes. The goal is to obtain the best possible solution for the time dependent instrumental gain while eliminating the detrimental phase fluctuations introduced by the ionosphere. The instrumental gain can be considered to have a global (on-axis) term in conjunction with a detailed spatial and spectral shape component. Some of the early LOFAR results discussed in RD6 have made use of some 500 relatively bright sources within the field to derive solutions in some 150 "directions" that represent a bundled collection of source locations. More recent results have apparently utilised up to 20,000 source components (including wavelets, Gaussians and delta functions) to more accurately represent the population within both the main beam and its sidelobes together with the complex morphologies of individual sources.

The most demanding requirements needed to achieve deep imaging performance with LOFAR (from Table 3) include:

1. A rather small systematic residual in the main beam asymmetry, $\underline{\varepsilon_Q}$ = 0.0005. The LOFAR team have invested significant effort in improvement of the station beam model and its systematic variation with time.
2. Extensive discrete source modelling within the first sidelobes of the station beam, down to $\underline{\varepsilon_S}$ = 0.001, is also predicted to be necessary. The first sidelobe of the LOFAR station beam has a solid angle of about 75 deg^2 at 120 MHz, so that the brightest random source is expected to have a flux density of about 3.6 Jy. All sources within the first sidelobe down to an apparent flux density of $\underline{S_{Min}} = S_{Max} \times \underline{\varepsilon_S}$ = 3.6 mJy should ultimately be included in the self-cal model. Since an actual peak sidelobe response of ε_S = 0.1 is likely, this would correspond to the 2300 or so sources with intrinsic flux density exceeding about 36 mJy (or $S_{1.4} \approx 5$ mJy) in this area.
3. A very high source modelling precision, ε_M = 0.002. The very large number of source components (50,000) currently being used for the most sensitive results seems to be qualitatively consistent with this requirement.

The far sidelobe depth that is predicted to be required by LOFAR to achieve thermal noise limited performance is $\underline{\eta_F}$ = 0.3. This implies an effective "all-sky" suppression level of $\underline{\varepsilon_F} = \underline{\eta_F}(\lambda/d)^2 = 2 \times 10^{-3}$ or -27 dB at an observing frequency of 120 MHz for individual visibilities. Since the measured sidelobe suppression factor is η_F = 0.5, or -25 dB at 120 MHz, this means that modelling down to $S_{1.4} > 860(\underline{\eta_F}/\eta_F)$ = 520 Jy, i.e. limited to only Cygnus A and Cas A should be sufficient for night-time observing in the event that the self-calibration makes effective use of the long baseline data (B_{Med} = 6.6km). Any reduction of B_{Med} will make this modelling requirement more stringent, as $B_{Med}^{-1.55}$.

5.4 SKA1-Low

The requirements for SKA1-Low are similar, but more stringent than, those derived for LOFAR-NL in Table 3. A very small systematic residual in the main beam asymmetry, $\underline{\varepsilon_Q}$ = 0.0004, must be achieved. This will need to build on the LOFAR experience and extend the dynamic modelling of station beam shapes to even higher precision. Discrete source modelling within the near-in sidelobes will also need to extend to about twice the depth noted above for LOFAR, including sources with apparent flux density (at 120 MHz) greater than about 1.5 mJy. With a peak sidelobe response of ε_S = 0.1, this represents about 3000 sources with intrinsic flux greater than 15 mJy (or $S_{1.4} \approx 2$ mJy) within the 60 deg^2 solid angle of the first sidelobe. The source modelling precision must also be improved by a factor of about two over LOFAR to $\underline{\varepsilon_M}$ = 0.001, which is comparable to the requirement for SKA1-Mid. Improved methods of source representation will likely need development, together with data comparison strategies that minimise time and frequency smearing effects.

The most challenging requirement noted in Table 3 is that on the far sidelobe suppression factor, $\underline{\eta_F}$ = 0.05. Figure 12 demonstrates that unlike many of the other requirements, which have a similar magnitude over much of the observing band, this constraint only becomes significant at the lowest frequencies. Achieving $\underline{\eta_F}$ = 0.05 at 50 MHz would require $\underline{\varepsilon_F} = \underline{\eta_F}(\lambda/d)^2$ = 1.5×10^{-3} or -28 dB. For an actual η_F = 0.5, or -18 dB, this corresponds to all-sky modelling of night-time observations down to $S_{1.4}$ > $860(\underline{\eta_F}/\eta_F)$ = 86 Jy. For a random pointing direction this encompasses about 5 – 10 discrete sources. The requirement relaxes to $\underline{\eta_F}$ = 0.14 at 100 MHz. At this higher frequency, modelling down to $S_{1.4}$ = $860(\underline{\eta_F}/\eta_F)$ = 240 Jy, that includes only 2 – 3 discrete sources, may already be sufficient. It will be challenging to reach the thermal noise floor in deep integrations at frequencies between 50 – 100 MHz.

We have considered how alternative station beam forming strategies might influence the calibration challenges facing SKA1-Low. To this end we have repeated the analysis outlined previously in Section 4.4, but instead simulate observations with both 512*6 = 3072 “sub-stations” (in Figure 13) and with 512/6 = 85 “super-stations” (in Figure 14). In all cases we preserve the total number (131,072) of antennas as well as the basic layout (which determines B_{Med} = 4.0 km).
All requirements, specifically: $\underline{\varepsilon_M}$, $\underline{\varepsilon_B}$, $\underline{\varepsilon_Q}$, $\underline{\varepsilon'_P}$, $\underline{\varepsilon_S}$ and $\underline{\eta_F}$ are significantly impacted by the choice of station diameter, in the sense that they are each relaxed by about 0.6 dex for a 14m station relative to a station of 35m. Conversely all requirements are aggravated by about 0.6 dex with an 86m station size. Sub-station correlations may be a very attractive scenario to consider, although there are far-reaching implications for the scale of the computational problem. To first order, the data transport and computing load will scale as the square of the number of stations being correlated. While beyond the scope of the current discussion to analyse in more detail, these implications will need to be carefully quantified.

Another means of relaxing the calibration requirements with a fixed total number of antennas is via a redistribution of the collecting area within the array configuration from the core to remote scales. Increasing the median baseline length from its current value B_{Med} = 4km to 10km would reduce the required precision by between 0.3 – 0.8 dex for the various parameters.
Other considerations that are of relevance to the far sidelobe performance include the fortuitous Northern location of Cygnus A ($\alpha,\delta = 20^h,+41°$) and Cas A ($\alpha,\delta = 23^h.5,+59°$), that together account for all discrete night-time source components with $S_{1.4}$ > 340 Jy. The Southern SKA1-Low site latitude of -27° implies that these two sources will only occasionally be above the horizon. Another positive consideration might be the spectral flattening at frequencies below about 100 MHz that applies to a subset of the discrete source population. Unfortunately, the bright tail of the source distribution is dominated by luminous extended doubles that only display a modest spectral flattening at low frequencies.

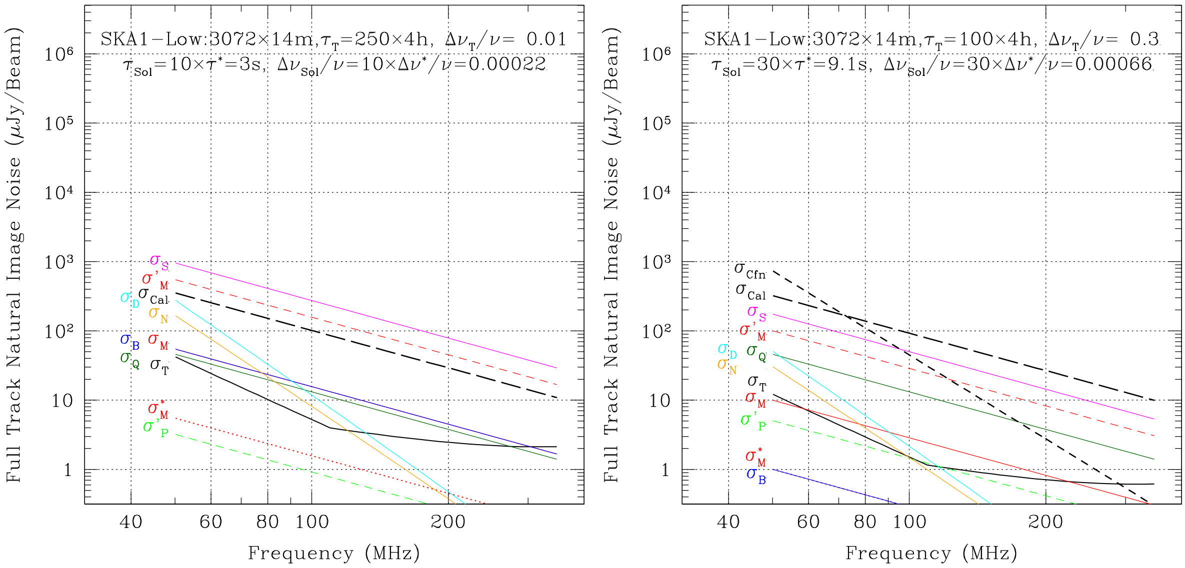

Figure 13. Noise error budget for a deep spectral line (left) and broad-band continuum (right) observation with SKA1-Low utilising "sub-station" correlation as function of observing frequency. The various error terms are colour coded and individually plotted.

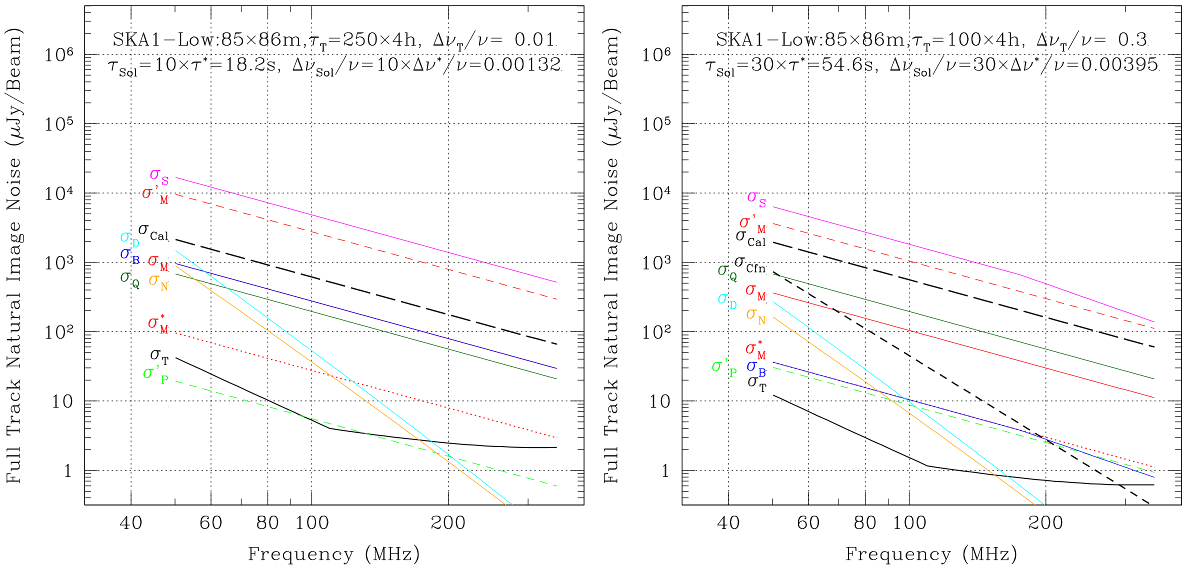

Figure 14. Noise error budget for a deep spectral line (left) and broad-band continuum (right) observation with SKA1-Low utilising "super-station" correlation as function of observing frequency. The various error terms are colour coded and individually plotted.

6 Requirements Budget

Up to this point we have considered each potential degradation to the image noise performance in isolation and quantified the approximate parameter values that reduce those contributions to the level of the thermal noise (as listed in Table 3). In practise, a combination of all these effects can be anticipated and yet the total noise should not be degraded beyond some acceptable limit. In the first instance we will adopt a total noise degradation factor, $\delta_N = 1.2$, and assume that this degradation is distributed equally amongst, $n_V = 6$, independent contributing factors. We can then calculate the required post-calibration parameter values that satisfy this condition and plot these as a function of the observing frequency. The method of calculation of the required parameters, $\underline{\varepsilon_i}$, is given by,

$$\underline{\varepsilon_i} = \varepsilon_i \, (\sigma_T / \sigma_i) \, [(\delta_N^2 - 1)/ n_V]^{1/2}$$

where ε_i is the assumed instrumental parameter from Table 2, and σ_T as well as σ_i are the thermal and error noise terms of the deep integrations plotted in Figures 6 and 12.

6.1 SKA1-Mid

The post-calibration requirements that apply to deep integrations with SKA1-Mid are illustrated in Figure 15. As already noted in §§ 4.21 and 4.22 above, it is the slowly varying systematic pointing errors, P, on timescales of τ_P = 15 minutes, that dominate over the rapidly varying ones, ε'_P, so we will only consider that dominant type of pointing error here. We plot $\underline{P_{deg}}$ in units of degrees (rather than arcsec) to permit multiple parameters to be overlaid on the same plot. The parameters $\underline{\varepsilon_S}$ and $\underline{\eta_F}$ refer to the near-in- and far- sidelobe response of the primary beam and the numerical values in the plots demonstrate the depth of the source populations within these regions that must be modelled, to the extent that they are more stringent than the intrinsic attributes of the antenna system, ε_S and η_F, from Table 2. The $\underline{\varepsilon_M}$ parameter pertains to the modelling precision of the discrete source population. For reference, source models consisting of discrete delta functions on a relatively coarse rectangular grid only provide a modelling precision of about $\varepsilon_M = 0.1$. Much more accurate source models will be needed to meet the requirements, $\underline{\varepsilon_M} = 10^{-3.5}$, shown in the Figures here. The parameter $\underline{\varepsilon_B}$ represents the level of residual (i.e. unmodelled) modulation of the primary beam gain with frequency, while $\underline{\varepsilon_Q}$ represents the level of residual (unmodelled) primary beam shape asymmetry at a fixed frequency.

The most stringent requirements are those associated with deep continuum observations. These will require a pointing calibration strategy that provides exceptionally low systematic pointing errors of about P = 0.1 arcsec at GHz frequencies. It is important to stress that only systematic pointing errors (namely those that would repeat from one sidereal day to the next) must be reduced to this level. The error budget is about 10 times more tolerant to slow pointing errors that vary randomly from one day to another. The primary beam shape and its frequency modulation must also be calibrated to a very high level of precision. Residual spectral gain modulations, $\underline{\varepsilon_B}$, and spatial asymmetries of the primary beam, $\underline{\varepsilon_Q}$, need to be kept below about 10^{-4} of the on-axis response. The discrete source population that must be incorporated into the self-calibration solutions corresponds to parameters $\underline{\varepsilon_S} = 10^{-4}$ within the near-in sidelobes of the station beam and $\underline{\eta_F} = 10^{-2}$ near 400 MHz within the far sidelobe response. Since the anticipated instrumental values are $\varepsilon_S = 0.01$ and $\eta_F = 0.2$ from Table 2, this implies that the brightest 2 dex of sources within the near-in sidelobes must be considered as well as about 1 dex of the all-sky source population at the lowest observing frequencies.

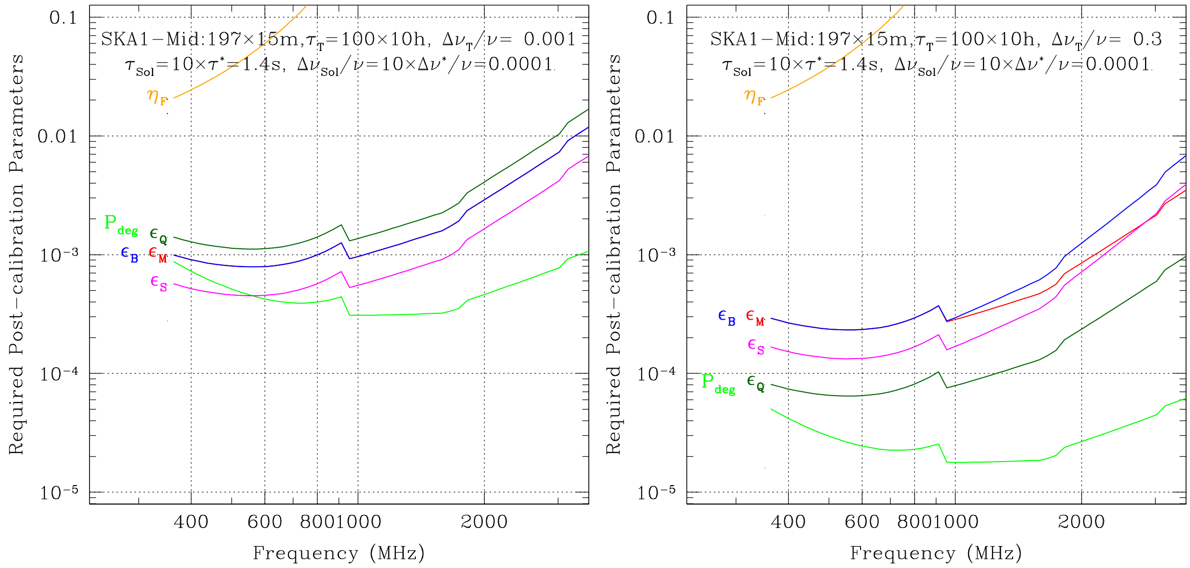

Figure 15. Requirements budget for a deep spectral line (left) and broad-band continuum (right) observation with SKA1-Mid as function of observing frequency. The various terms are colour coded and individually plotted. The thermal noise degradation, $\delta_N = 1.2$, is distributed equally over $n_V = 6$ random contributions.

6.2 SKA1-Low

Post-calibration requirements that apply to deep integrations with SKA1-Low are illustrated in Figure 16. As noted previously in § 4.4.2, and illustrated in Figure 12, the broad-band continuum noise floor will be determined by source confusion noise over most of the band. Nonetheless, the requirements have a similar magnitude for both the spectral and broad-band applications, as is apparent from Figure 16. For SKA1-Low there is assumed to be no slowly varying pointing error, but only the rapidly varying electronic pointing error that leads to an induced gain error of magnitude ε'_P on the flanks of the station beam. The constraint on residual pointing errors of this type is only moderately demanding, amounting to $\underline{\varepsilon'_P} = 10^{-3}$. The requirements on residual spectral gain modulations, $\underline{\varepsilon_B}$, and spatial asymmetries of the station beam, $\underline{\varepsilon_Q}$, are very similar to those identified for SKA1-Mid, namely between $10^{-3.5}$ and 10^{-4} of the on-axis response. Source modelling precision must also be similarly high, $\underline{\varepsilon_M} \approx 10^{-3.5}$. The discrete source population that must be incorporated into the self-calibration solutions corresponds to parameters $\underline{\varepsilon_S} = 10^{-4}$ near 100 MHz within the near-in sidelobes of the station beam and $\underline{\eta_F} = 10^{-3}$ near 50 MHz within the far sidelobe response. Since the anticipated instrumental values $\varepsilon_S = 0.1$ and $\eta_F = 0.5$ from Table 2 are relatively high, this implies that the brightest 3 dex of sources within the near-in sidelobes and 2.5 dex of the all-sky source population must be considered.

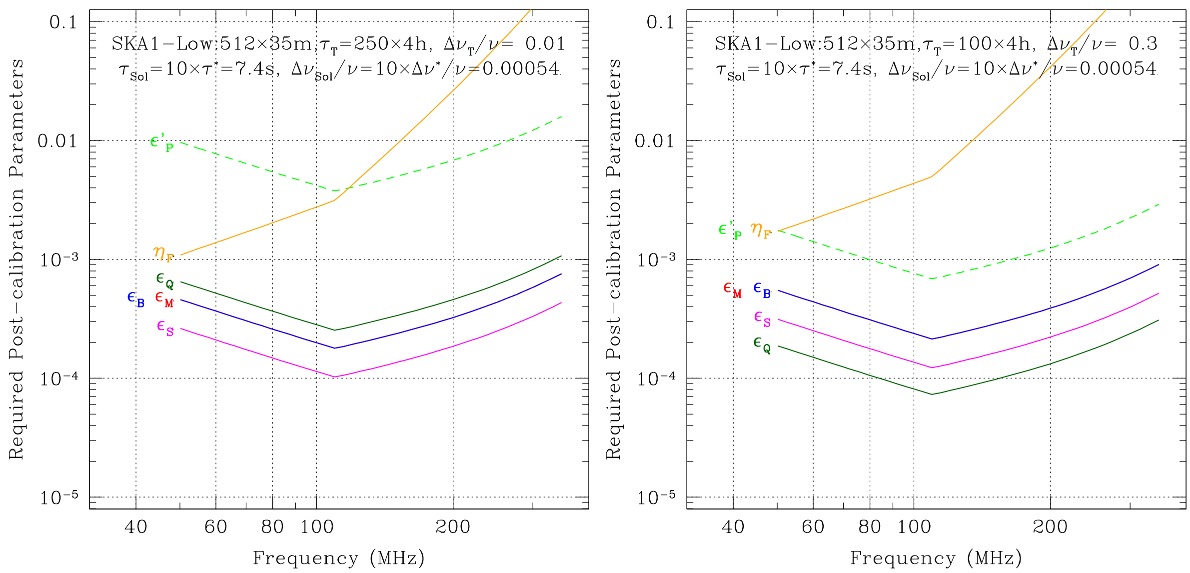

Figure 16. Requirements budget for a deep spectral line (left) and broad-band continuum (right) observation with SKA1-Low as function of observing frequency. The various error terms are colour coded and individually plotted. The thermal noise degradation, δ_N = 1.2, is distributed equally over n_V = 6 random contributions.